

# $\alpha$ particle preformation in heavy nuclei and penetration probability

H.F. Zhang<sup>1</sup> and G. Royer<sup>2\*</sup>

<sup>1</sup> *School of Nuclear Science and Technology, Lanzhou University, Lanzhou 730000, People's Republic of China and*

<sup>2</sup> *Laboratoire Subatech, UMR: IN2P3/CNRS-Université-Ecole des Mines, 44307 Nantes Cedex 03, France*

(Dated: March 12, 2022)

The  $\alpha$  particle preformation in the even-even nuclei from  $^{108}\text{Te}$  to  $^{294}118$  and the penetration probability have been studied. The isotopes from Pb to U have been firstly investigated since the experimental data allow to extract the microscopic features for each element. The assault frequency has been estimated using classical methods and the penetration probability from tunneling through the Generalized Liquid Drop Model (GLDM) potential barrier. The preformation factor has been extracted from experimental  $\alpha$  decay energies and half-lives. The shell closure effects play the key role in the  $\alpha$  preformation. The more the nucleon number is close to the magic numbers, the more the formation of  $\alpha$  cluster is difficult inside the mother nucleus. The penetration probabilities reflect that 126 is a neutron magic number. The penetration probability range is very large compared to that of the preformation factor. The penetration probability determines mainly the  $\alpha$  decay half-life while the preformation factor allows to obtain information on the nuclear structure. The study has been extended to the newly observed heaviest nuclei.

PACS numbers: 23.60.+e, 21.10.Jx, 27.90.+b

## I. INTRODUCTION

The  $\alpha$  emission is one of the decay channels of the heavy nuclei. Measurements on the  $\alpha$  decay can provide reliable information on the nuclear structure such as the ground-state energy, the ground-state half-life, the nuclear spin and parity, the nuclear deformation, the nuclear clustering, the shell effects and the nuclear interaction [1, 2, 3, 4, 5, 6, 7, 8, 9, 10, 11, 12]. Measurements on the  $\alpha$  decay are also used to identify new nuclides or new heavy elements since the  $\alpha$  decay allows to extract clear and reliable information on the parent nucleus [13, 14, 15]. Recently, the interest in the  $\alpha$  decay has been renewed because of the development of radioactive beams and new detector technology under low temperature.

The  $\alpha$  decay process was first explained by Gamow and by Condon and Gurney in the 1920s [16, 17] as a quantum-tunneling effect and is one of the first examples proving the need to use the quantum mechanics to describe the nuclear phenomena and its correctness. Later on, theoretical calculations were performed to predict the absolute  $\alpha$  decay width, to extract nuclear structure information, and to pursue a microscopic understanding of the  $\alpha$ -decay phenomenon. These studies are based on various theoretical models such as the shell model, the fissionlike model, and the cluster model [18, 19, 20, 21, 22, 23, 24, 25, 26, 27, 28, 29, 30]. In the  $\alpha$  cluster model, the decay constant  $\lambda$  is the product of three terms: the cluster preformation probability  $P_0$ , the assault frequency  $\nu_0$  and the barrier penetrability  $P$ . The  $\alpha$  particle emission is a quantum tunnelling through the potential barrier leading from the mother nucleus to the two emitted fragments: the  $\alpha$  particle and

the daughter nucleus. The penetrability can be described successfully using the WKB approximation. The most important problem of the  $\alpha$  decay is how to estimate the preformation probability  $P_0$  that the  $\alpha$  particle exists as a recognizable entity inside the nucleus before its emission. It is very dependent on the structure of the states of the mother and daughter nuclei and is a measure of the degree of resemblance between the initial state of the mother nucleus and the final state of the daughter nucleus plus the  $\alpha$  particle. Within an asymmetric fission picture the preformation factor  $P_0$  has been taken as 1 in previous studies and that allows to reproduce the experimental  $\alpha$  decay half-lives [22, 26] when the experimental  $Q_\alpha$  values are used. There are, however, still small differences between the calculated and experimental values and these discrepancies may be used to determine the  $\alpha$ -preformation probability. The  $\alpha$  preformation factor is very important from the viewpoint of the nuclear structure. Numerous studies of the  $\alpha$  decay have been concentrated on this problem [31, 32, 33, 34, 35, 36, 37, 38]. There are also several approaches to calculate the formation amplitude : the shell model, the BCS method [39], the hybrid (shell model+ $\alpha$ -cluster) model [40] etc. The effect of continuum states on the  $\alpha$  decay is known to be very large [39]. One needs therefore very large shell model basis to obtain the experimental values of the  $\alpha$ -preformation probability. The hybrid model [40], which treats a large shell model basis up to the continuum states through the wavefunction of the spatially localized  $\alpha$  cluster, explains well the experimental decay width. In these calculations the wave function is necessary, and it is not easy to extend the approaches for nuclei including more nucleons outside the double-magic core.

In this contribution, the preformation factor is extracted from the experimental  $\alpha$  decay half-life  $T_\alpha$  and the penetration probability is obtained from the WKB approximation. The potential barrier is determined within a generalized liquid drop model (GLDM) includ-

---

\*Electronic address: royer@subatech.in2p3.fr

ing the proximity effects between the  $\alpha$  particle and the daughter nucleus and adjusted to reproduce the experimental  $Q_\alpha$  [22, 26].

The paper is organized as follows. In Sec. 2, the methods for calculating the assault frequencies, the penetrability of the even-even nuclei and the preformation factor are presented. The calculated results are shown and discussed in Sec. 3. In the last section, the conclusions are given and future works are proposed.

## II. METHODS

The  $\alpha$  decay constant is defined as

$$\lambda = P_0 \nu_0 P. \quad (1)$$

Imagining the  $\alpha$  particle moving back and forth inside the nucleus with a velocity  $v = \sqrt{\frac{2E_\alpha}{M}}$ , it presents itself at the barrier with a frequency :

$$\nu_0 = \left( \frac{1}{2R} \sqrt{\frac{2E_\alpha}{M}} \right). \quad (2)$$

$R$  is the radius of the parent nucleus given by

$$R_i = (1.28A_i^{1/3} - 0.76 + 0.8A_i^{-1/3}) \text{ fm}, \quad (3)$$

and  $E_\alpha$  is the energy of the alpha particle, corrected for recoil;  $M$  being its mass.

The penetration probability  $P$  is calculated within the WKB approximation. The potential barrier governing the  $\alpha$  emission is determined within the GLDM, including the volume, surface, Coulomb and proximity energies [41]:

$$E = E_V + E_S + E_C + E_{\text{Prox}}. \quad (4)$$

When the nuclei are separated:

$$E_V = -15.494 [(1 - 1.8I_1^2)A_1 + (1 - 1.8I_2^2)A_2] \text{ MeV}, \quad (5)$$

$$E_S = 17.9439 [(1 - 2.6I_1^2)A_1^{2/3} + (1 - 2.6I_2^2)A_2^{2/3}] \text{ MeV}, \quad (6)$$

$$E_C = 0.6e^2 Z_1^2/R_1 + 0.6e^2 Z_2^2/R_2 + e^2 Z_1 Z_2/r, \quad (7)$$

where  $A_i$ ,  $Z_i$ ,  $R_i$  and  $I_i$  are the mass numbers, charge numbers, radii and relative neutron excesses of the two nuclei.  $r$  is the distance between the mass centres. The radii  $R_i$  are given by Eq. (3).

For one-body shapes, the surface and Coulomb energies are defined as [22, 41]:

$$E_S = 17.9439(1 - 2.6I^2)A^{2/3}(S/4\pi R_0^2) \text{ MeV}, \quad (8)$$

$$E_C = 0.6e^2(Z^2/R_0) \times 0.5 \int (V(\theta)/V_0)(R(\theta)/R_0)^3 \sin \theta d\theta. \quad (9)$$

$S$  is the surface of the one-body deformed nucleus.  $V(\theta)$  is the electrostatic potential at the surface and  $V_0$  the surface potential of the sphere.

The surface energy results from the effects of the surface tension forces in a half space. When there are nucleons in regard in a neck or a gap between separated fragments an additional term called proximity energy must be added to take into account the effects of the nuclear forces between the close surfaces. This term is essential to describe smoothly the one-body to two-body transition and to obtain reasonable fusion barrier heights. It moves the barrier top to an external position and strongly decreases the pure Coulomb barrier.

$$E_{\text{Prox}}(r) = 2\gamma \int_{h_{\text{min}}}^{h_{\text{max}}} \Phi [D(r, h)/b] 2\pi h dh, \quad (10)$$

where  $h$  is the distance varying from the neck radius or zero to the height of the neck border.  $D$  is the distance between the surfaces in regard and  $b = 0.99$  fm the surface width.  $\Phi$  is the proximity function. The surface parameter  $\gamma$  is the geometric mean between the surface parameters of the two fragments. The combination of the GLDM and of a quasi-molecular shape sequence has allowed to reproduce the fusion barrier heights and radii, the fission and the  $\alpha$  and cluster radioactivity data.

The barrier penetrability  $P$  is calculated within the action integral

$$P = \exp\left[-\frac{2}{\hbar} \int_{R_{\text{in}}}^{R_{\text{out}}} \sqrt{2B(r)(E(r) - E(\text{sphere}))} \right]. \quad (11)$$

The deformation energy (relatively to the sphere energy) is small till the rupture point between the fragments [22] and the two following approximations may be used :  $R_{\text{in}} = R_d + R_\alpha$  and  $B(r) = \mu$  where  $\mu$  is the reduced mass.  $R_{\text{out}}$  is simply  $e^2 Z_d Z_\alpha / Q_\alpha$ .

The decay constant may be deduced from the experimental  $\alpha$  decay half-life  $T_\alpha$  by

$$\lambda = \frac{\ln 2}{T_\alpha}. \quad (12)$$

The preformation factor  $P_0$  of an  $\alpha$  cluster inside the mother nucleus can be estimated inserting Eq.(2), Eq.(11) and Eq.(12) in Eq.(1).

## III. RESULTS AND DISCUSSIONS

The values of the decay constant  $\lambda$ , the velocity, the assault frequency  $\nu_0$ , the penetrability  $P$  and the preformation factor  $P_0$  are given for the even-even Pb, Po, Rn, Ra, Th and U isotopes in the tables 1 and 2.

In the simple picture of an  $\alpha$  particle moving with a kinetic energy  $E_\alpha$  inside the nucleus, the order of magnitude of the  $\alpha$  velocity  $v$  is  $1.0 \times 10^{22}$  fm/s for all considered nuclei. The order of magnitude of the assault frequency

$\nu_0$  calculated by Eq.(1) is  $1.0 \times 10^{21} s^{-1}$  both in the table 1 and the table 2. The variations of  $\nu$  and  $\nu_0$  are small. In the previous study relative to the  $\alpha$  decay half-lives using the GLDM [22], the assault frequency  $\nu_0$  is fixed as  $1.0 \times 10^{20}$ , which is smaller by one order of magnitude than the value obtained in the present calculation, meaning that an averaged preformation factor of 0.1 has been included in the previous  $\alpha$  decay study. So the previous calculations are consistent quantitatively with the experimental data in general. A fixed value of the assault frequency cannot describe the detailed features of the nuclear structure and the last column of the tables 1 and 2 displays the extracted preformation factor  $P_0$  when the Eq. (2) is assumed. To study the correlation between the preformation factors and the structure properties, the preformation factors of Pb, Po, Rn, Ra, Th, and U isotopes are given as a function of the neutron number  $N$  in Fig.1. The preformation factors of the isotopes generally decrease with increasing neutron number up to the spherical shell closure  $N=126$ , where the minimum of  $P_0$  occurs, and then they increase quickly with the neutron number. The values of the preformation factors is always minimum for the Po, Rn, Ra, Th, and U isotopes when  $N=126$ . The preformation factors of  $N=126$  isotones are shown in Fig. 2. The preformation factors increase when the proton number goes away from the magic number  $Z=82$ . The maximum values of the preformation factor for the five elements, which correspond to the most neutron-rich nucleus from Po to U isotopes respectively, are presented in Fig.3. In general, the values increase with the proton number. From  $^{232}\text{Th}$  to  $^{238}\text{U}$ , the value of the preformation factor decreases apparently, even if the proton number  $Z$  is far from the magic number  $Z=82$ . The neutron number of  $^{238}\text{U}$  ( $N=146$ ) is closer to the sub-magic neutron number  $N=152$  than that of the nucleus  $^{232}\text{Th}$  ( $N=142$ ); so the preformation factor of  $^{232}\text{Th}$  is larger than that of the nucleus  $^{238}\text{U}$ . As a conclusion the shell closure effects play the key role in the  $\alpha$  formation mechanism. The more the nucleon number is close to the magic numbers, the more the formation of the  $\alpha$  cluster inside the mother nucleus is difficult.

The ground-state spin and parity of even-even nuclei is  $0^+$  and the  $\alpha$  decay of even-even nuclei mainly proceeds to the ground state of the daughter nucleus. Though the parent nucleus may also decay to the excited states of the daughter nucleus, the probability is very small and it can be neglected for a systematic study of penetrability. The calculated penetrabilities are given in the seventh column in the tables 1 and 2. The values of the penetrability vary in a wide range from  $10^{-39}$  to  $10^{-14}$  for the even-even isotopes of Pb, Po, Rn, Ra, Th, and U, implying that the penetrability plays the key role to determine the  $\alpha$  decay half-lives. The values of  $\log_{10}(P)$  are plotted in Fig. 4 for the even-even Pb, Po, Rn, Ra, Th, and U isotopes. They decrease with the increasing neutron number  $N$  for the Pb, Po, Rn, Ra, and Th isotopes before the magic number  $N=126$ . For the U isotopes, the experimental data of  $Q_\alpha$  and  $T_\alpha$  are not supplied. The penetrability values

increase sharply after  $N=126$  and reach the maximum at  $N=128$ , then they decrease again quickly for Po, Rn, Ra, Th, and U isotopes. For the Pb isotopes the experimental data of  $Q_\alpha$  and  $T_\alpha$  are not supplied after  $N=128$ . For the nuclei with two neutrons outside the closed shell, the  $\alpha$  particle emission is easier than that of the other nuclei of the same isotopes. The closed shell structures play also the key role for the penetrability mechanism. The more the nucleon number is far away from the nucleon magic numbers, the more the penetrability of the  $\alpha$  cluster from mother nucleus becomes larger.

The values of the  $\alpha$  decay constant  $\lambda$  deduced from the experimental half-lives are shown in the fourth column of the tables 1 and 2 for the even-even isotopes of Pb, Po, Rn, Ra, Th, and U. In order to clarify the relations between the decay constant  $\lambda$ , the preformation factor  $P_0$ , the assault frequency  $\nu_0$  and the penetrability  $P$ , the values of  $\log_{10}(P_0)$ ,  $\log_{10}(\nu_0)$ ,  $\log_{10}(P)$ , and  $\log_{10}(\lambda)$  are displayed as functions of the neutron number  $N$  for Po isotopes in the Fig. 5. The curve shape of  $\log_{10}(\lambda)$  is the same as that of  $\log_{10}(P)$ , confirming that the  $\alpha$  decay half-lives are mainly decided by the penetrability.  $\log_{10}(\nu_0)$  decreases smoothly before  $N=126$ , increases from  $N=126$  to  $N=128$ , and decreases again with the increasing of the neutron number, indicating that the assault frequency of  $\alpha$  particle can also reflect the shell effects, even if  $\log_{10}(P_0)$  exhibits the microscopic nuclear structure more clearly.

It has been shown that the nuclear structure characteristics can be detected through the study of the  $\alpha$  formation and penetrability in the above discussions. It is tempting to extend the study to the superheavy nuclei. Recently, isotopes of the elements 112, 113, 114, 115, 116 and 118 have been synthesized in fusion-evaporation reactions using  $^{209}\text{Bi}$ ,  $^{233,238}\text{U}$ ,  $^{242,244}\text{Pu}$ ,  $^{243}\text{Am}$ ,  $^{245,248}\text{Cm}$  and  $^{249}\text{Cf}$  targets with  $^{48}\text{Ca}$  and  $^{70}\text{Zn}$  beams [13, 14, 15]. These recent experimental results have led to new theoretical studies on the  $\alpha$  decay; for example within the relativistic mean field theory [42], the DDM3Y interaction [25], the GLDM [26, 43] and the Skyrme-Hartree-Fock mean field model [30]. All the above theoretical works are concentrated on the half-lives of these observed superheavy nuclei, and the results are reasonably consistent with the experimental data. The characteristics of the  $\alpha$  formation and penetrability for the even-even superheavy nuclei are listed in the table 3. The preformation factors are distributed between 0.005 and 0.05 showing that the shell effect structures are also important features for the superheavy nuclei. The preformation factor of  $^{294}118$  is 0.0056, which is smaller than that of the spherical nucleus  $^{210}\text{Po}$ , implying perhaps that the neutron number  $N=176$  is a submagic number. In Ref. [44], it is also pointed out that for the oblate deformed chain of  $Z=112$ , the shell closure appears at  $N=176$ . Thus the preformation of  $\alpha$  is not easy for these heaviest nuclei. The penetration probabilities  $P$  given in the seventh column of the table 3 always stay between  $10^{-20}$  and  $10^{-15}$ . The penetration probabilities are relatively very large, while the range is

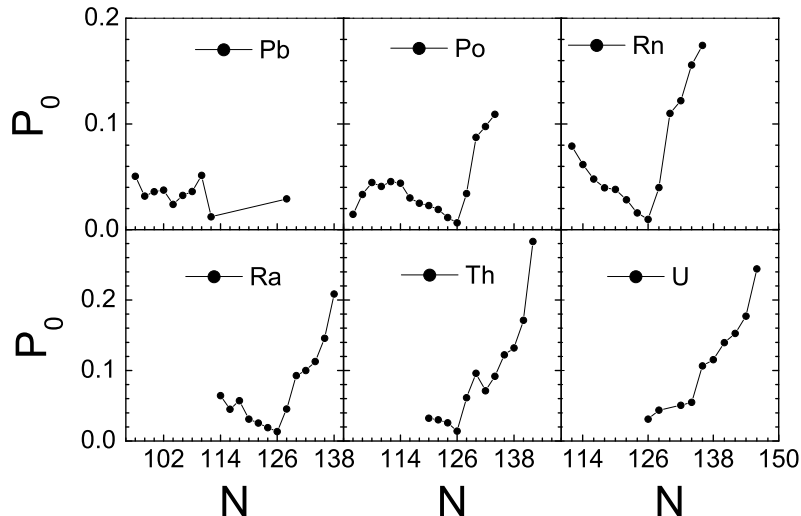


FIG. 1: Extracted preformation factors for the even-even isotopes of Pb, Po, Rn, Ra, Th, and U.

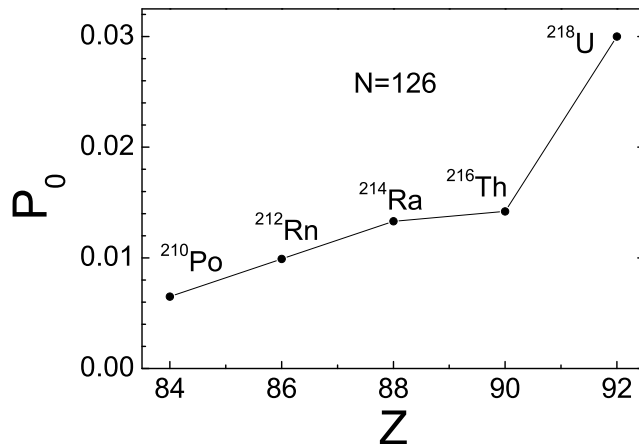


FIG. 2: Extracted preformation factors for the  $N=126$  isotones of Po, Rn, Ra, Th, and U.

narrow. So it is easy for the  $\alpha$  particle to escape from these heaviest nuclei as soon as they form, confirming that the superheavy nuclei are weakly bound.

The experimental but model-dependent preformation factors of the 180 even-even nuclei from  $Z=52$  to  $Z=118$  are displayed in Fig. 6. In general, the formation factor decreases with the increase of the mass number  $A$ . It can be understood easily that the theoretical  $\alpha$  decay GLDM half-lives are very slightly higher than the experimental data for the light nuclei and lower for the heaviest systems, when the preformation factors are neglected. The preformation factors decrease with mass number till about 210, then, the preformation factors jump nearly

one order of magnitude, and finally decrease again, due to the neutron number  $N=126$  in this mass region.

#### IV. CONCLUSION AND OUTLOOK

A global study of the  $\alpha$  formation and penetration is presented for the even-even nuclei from  $Z=52$  to  $Z=118$ . The decay constants are obtained from the experimental half-lives. The penetration probabilities are calculated from the WKB approximation and the penetration barriers are constructed with the GLDM. After using a classical method to estimate the assault frequencies the

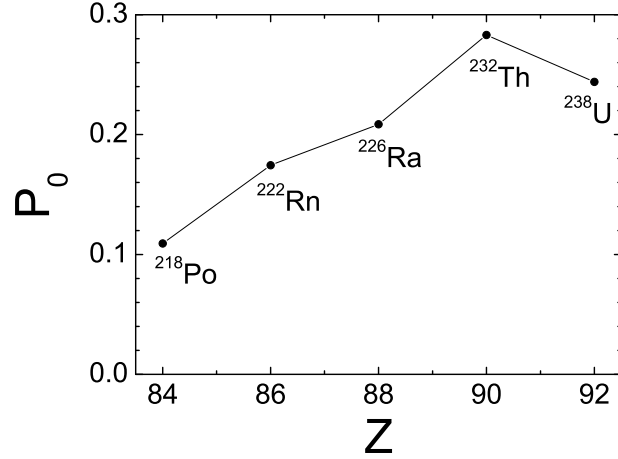


FIG. 3: Extracted preformation factors for  $^{218}\text{Po}$ ,  $^{222}\text{Rn}$ ,  $^{226}\text{Ra}$ ,  $^{232}\text{Th}$ , and  $^{238}\text{U}$ .

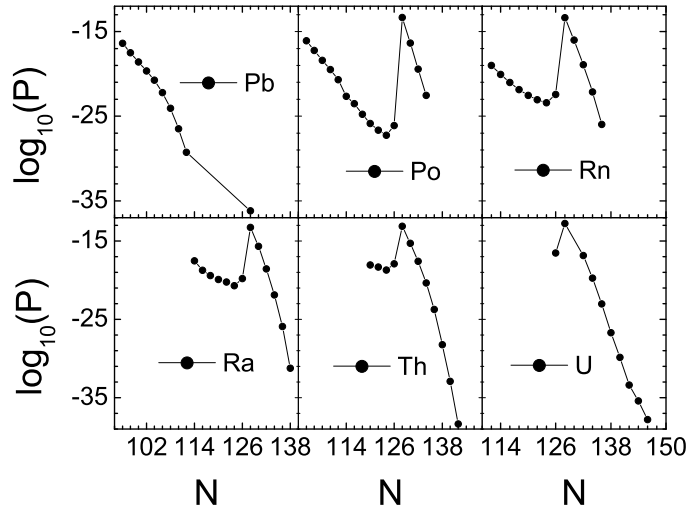


FIG. 4: Logarithms of the penetrability for the even-even isotopes of Pb, Po, Rn, Ra, Th, and U.

preformation factors are extracted systematically. The preformation factors are not constant for these nuclei, and show regular law for the studied isotopes. Clearly the closed shell structures play the key role for the preformation mechanism, and the more the nucleon number is close to the magic nucleon numbers, the more the preformation of  $\alpha$  cluster is difficult inside the mother nucleus. The decay constant is the product of the preformation, the penetration, and the assault frequency. The penetrability determines mainly the behaviour of the decay constant. The study is extended to the even-even super-heavy nuclei. The penetration probabilities are relatively very large and its range is narrow for the heaviest nuclei.

So it is easy for the  $\alpha$  particle to escape from these nuclei as soon as they are formed, confirming that the super-heavy nuclei are weakly bound. Thus, it is interesting and timely to study the preformation factors microscopically and systematically. It is also desired to extend the study to the odd  $A$  and odd-odd nuclei and extract possibly analytical formulas of preformation factors, which should be functions of the nucleon numbers and the  $\alpha$  decay energy. It would be also important to take into account the deformations, which may change the results by perhaps one order of magnitude.

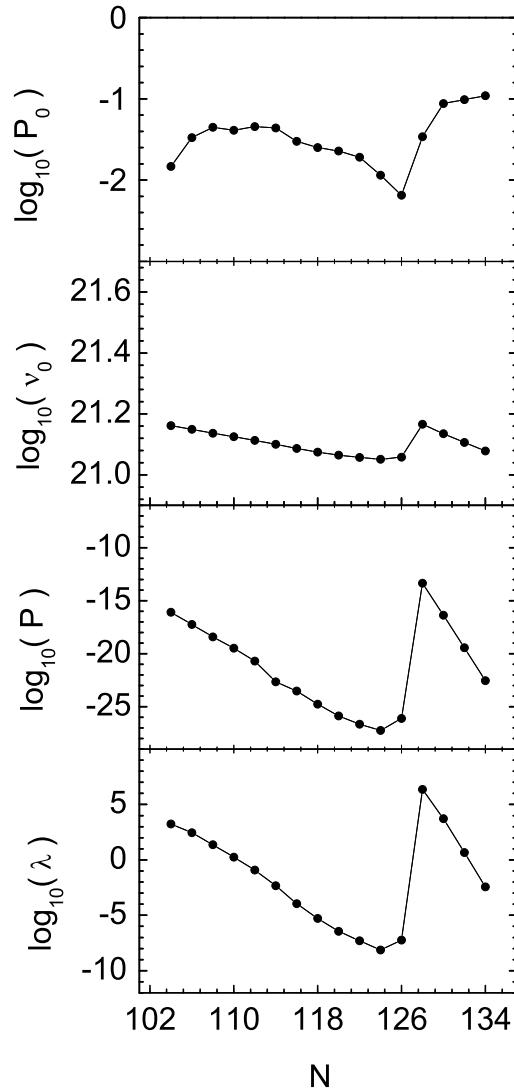


FIG. 5: Characteristics of the  $\alpha$  formation and penetration for the even-even Po isotopes.

## V. ACKNOWLEDGMENTS

H.F. Zhang is thankful to Prof. Bao-Qiu Chen, Zhong-Zhou Ren, En-Guang Zhao for valuable discussions. The work of H.F. Zhang was supported by the National Natural Science Foundation of China

(10775061,10505016,10575119,10175074), the Knowledge Innovative Project of CAS (KJCX3-SYW-N2), the Major Prophase Research Project of Fundamental Research of the Ministry of Science and Technology of China (2007CB815004).

- 
- [1] Z. Ren and G. Xu, Phys. Rev. **C 36**, 456 (1987).  
 [2] H. Horiuchi, Nucl. Phys. **A522**, 257c (1991).  
 [3] R.B. Firestone, V. S. Shirley, C. M. Baglin, S. Y. Frank Chu, and J. Zipkin, Table of Isotopes, 8th ed. (Wiley Interscience, New York, 1996).  
 [4] R. G. Lovas, R. J. Liotta, A. Insolia, K. Varga, and D. S. Delion, Phys. Rep. **294**, 265 (1998).

- [5] F. Garcia, O. Rodriguez, M. Gonçaves, S.B. Duarte, O.A.P. Tavares, and F. Guzman, J. Phys. **G 26**, 755 (2000).  
 [6] G. Audi, O. Bersillon, J. Blachot, and A.H. Wapstra, Nucl. Phys. **A729**, 3 (2003).  
 [7] T. N. Ginter, et al., Phys. Rev. **C 67**, 064609 (2003).  
 [8] P. E. Hodgson and E. Betak, Phys. Rep. **374**, 1 (2003).

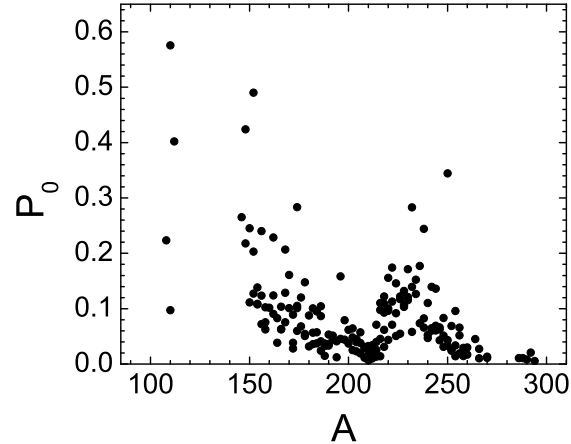


FIG. 6:  $\alpha$  preformation factors for 180 even-even nuclei ( $Z=52-118$ ).

- [9] R.-D. Herzberg, *J. Phys.* **G 30**, R123 (2004).
- [10] Z. G. Gan, J. S. Guo, X. L. Wu, Z. Qin, H. M. Fan, X. G. Lei, H. Y. Liu, B. Guo, H. G. Xu, R. F. Chen, C. F. Dong, F. M. Zhang, H. L. Wang, C. Y. Xie, Z. Q. Feng, Y. Zhen, L. T. Song, P. Luo, H. S. Xu, X. H. Zhou, G. M. Jin, and Z. Ren, *Eur. Phys. J.* **A 20**, 385 (2004).
- [11] D. Seweryniak *et al.*, *Phys. Rev.* **C 73**, 061301(R) (2006).
- [12] A.P. Leppänen *et al.*, *Phys. Rev.* **C 75**, 054307 (2007).
- [13] Yu.Ts. Oganessian *et al.*, *Phys. Rev.* **C 72**, 034611 (2005); *Phys. Rev.* **C 74**, 044602 (2006); *Phys. Rev.* **C 76**, 011601(R) (2007).
- [14] S. Hofmann *et al.*, *Eur. Phys. J.* **A 32**, 251 (2007).
- [15] K. Morita *et al.*, *J. Phys. Soc. Jpn* **76**, 045001 (2007).
- [16] G. Gamov, *Z. Phys.* **51**, 204 (1928).
- [17] E. U. Condon and R. W. Gurney, *Nature* **122**, 439 (1928).
- [18] D.N. Poenaru and M. Ivascu, *Rev. Roum. Phys.* **28**, 309 (1983).
- [19] B. A. Brown, *Phys. Rev.* **C 46**, 811 (1992).
- [20] K. Varga, R.G. Lovas, and R.J. Liotta, *Phys. Rev. Lett.* **69**, 37 (1992).
- [21] B. Buck, A. C. Merchant, and S. M. Perez, *At. Data Nucl. Data Tables* **54**, 53 (1993).
- [22] G. Royer, *J. Phys.* **G 26**, 1149 (2000); G. Royer and R. Moustabchir, *Nucl. Phys.* **A683**, 182 (2001).
- [23] R. K. Gupta *et al.*, *Phys. Rev.* **C 65**, 024601 (2002).
- [24] S. B. Duarte *et al.*, *At. Data Nucl. Data Tables* **80**, 235 (2002).
- [25] D. N. Basu, *Phys. Lett.* **B 566**, 90 (2003); P. Roy Chowdhury, D. N. Basu, and C. Samanta, *Phys. Rev. C* **75**, 047306 (2007).
- [26] H.F. Zhang, W. Zuo, J.Q. Li, and G. Royer, *Phys. Rev.* **C 74**, 017304 (2006); H.F. Zhang and G. Royer, *Phys. Rev.* **C 76**, 047304 (2007).
- [27] P. Mohr, *Phys. Rev.* **C 73**, 031301(R) (2006).
- [28] C. Xu and Z.Z. Ren, *Phys. Rev.* **C 74**, 014304 (2006); C. Xu and Z.Z. Ren, *Nucl. Phys.* **A760**, 303 (2005).
- [29] D.N. Poenaru, I.H. Plonski, and W. Greiner, *Phys. Rev.* **C 74**, 014312 (2006).
- [30] J.C. Pei, F.R. Xu, Z.J. Lin, and E.G. Zhao, *Phys. Rev.* **C 76**, 044326 (2007).
- [31] H.J. Mang, *Phys. Rev.* **119**, 1069 (1960).
- [32] A. Arima and S. Yoshida, *Nucl. Phys.* **A219**, 475 (1974).
- [33] T. Fliessback and H.J. Mang, *Nucl. Phys.* **A263**, 75 (1976).
- [34] Y.K. Gambhir, P. Ring, and P. Schück, *Phys. Rev. Lett.* **51**, 1235 (1983).
- [35] G.G. Dussel, A.J. Fendrik, and C. Pomar. *Phys. Rev.* **C 34**, 1969 (1986).
- [36] Z. Ren and G. Xu, *Phys. Rev.* **C 38**, 1078 (1988).
- [37] G. Röpke, A. Schnell, and P. Schück, *Phys. Rev. Lett.* **80**, 3177 (1998).
- [38] M. Hasega and K. Kaneko, *Phys. Rev.* **C 61**, 037306 (2000); K. Kaneko and M. Hasegawa, *Phys. Rev.* **C 67**, 041306 (2003).
- [39] D. S. Delion, A. Insolia, and R. J. Liotta, *Phys. Rev.* **C 54**, 292(1996); D. S. Delion, A. Sandulescu, and W. Greiner, *Phys. Rev.* **C 69**, 044318 (2004); D. S. Delion, R. J. Liotta, and R. Wyss, *Phys. Rev.* **C 76**, 044301 (2007).
- [40] K. Varga, R. G. Lovas, and R. J. Liotta, *Nucl. Phys.* **A550**, 421(1992).
- [41] G. Royer and B. Remaud, *Nucl. Phys.* **A444**, 477 (1985).
- [42] M. M. Sharma, A. R. Farhan, and G. Münzenberg, *Phys. Rev.* **C 71**, 054310 (2005).
- [43] G. Royer and H.F. Zhang, *Phys. Rev.* **C 77**, 037602 (2008).
- [44] X. H. Zhong, L. Li, P. Z. Ning, arXiv: nucl-th/0410083 (2003).

TABLE I: Characteristics of the  $\alpha$  formation and penetration for the even-even Pb, Po and Rn isotopes. The first column indicates the mother nucleus. The second and third columns correspond, respectively, to the experimental  $Q_\alpha$  and  $\log_{10}[T_\alpha(s)]$ . The fourth column is the decay constant  $\lambda$ . The fifth and sixth columns correspond, respectively, to the velocity and frequency of the  $\alpha$  cluster inside the mother nucleus. The seventh column is the penetration probability and the last column gives the preformation factor extracted from Eq. (1) and the data of this table.

<i>Nuclei</i>	$Q_\alpha$ [MeV]	$\log_{10}(T_\alpha)$	$\lambda[s^{-1}]$	$v[fm/s]$	$\nu_0[s^{-1}]$	P	$P_0$
$^{178}_{82}\text{Pb}$	7.790	-3.64	$3.012 \times 10^3$	$1.913 \times 10^{22}$	$1.453 \times 10^{21}$	$4.097 \times 10^{-17}$	0.0506
$^{180}_{82}\text{Pb}$	7.415	-2.30	$1.386 \times 10^2$	$1.816 \times 10^{22}$	$1.415 \times 10^{21}$	$3.098 \times 10^{-18}$	0.0317
$^{182}_{82}\text{Pb}$	7.080	-1.26	$1.261 \times 10^1$	$1.823 \times 10^{22}$	$1.347 \times 10^{21}$	$2.558 \times 10^{-19}$	0.0359
$^{184}_{82}\text{Pb}$	6.774	-0.21	$1.137 \times 10^0$	$1.784 \times 10^{22}$	$1.339 \times 10^{21}$	$2.262 \times 10^{-20}$	0.0375
$^{186}_{82}\text{Pb}$	6.470	1.08	$5.779 \times 10^{-2}$	$1.743 \times 10^{22}$	$1.303 \times 10^{21}$	$1.845 \times 10^{-21}$	0.0240
$^{188}_{82}\text{Pb}$	6.109	2.43	$2.569 \times 10^{-3}$	$1.694 \times 10^{22}$	$1.262 \times 10^{21}$	$6.264 \times 10^{-23}$	0.0325
$^{190}_{82}\text{Pb}$	5.697	4.26	$3.853 \times 10^{-5}$	$1.636 \times 10^{22}$	$1.214 \times 10^{21}$	$8.784 \times 10^{-25}$	0.0361
$^{192}_{82}\text{Pb}$	5.221	6.56	$1.927 \times 10^{-7}$	$1.566 \times 10^{22}$	$1.157 \times 10^{21}$	$3.237 \times 10^{-27}$	0.0514
$^{194}_{82}\text{Pb}$	4.738	9.99	$7.077 \times 10^{-11}$	$1.491 \times 10^{22}$	$1.098 \times 10^{21}$	$5.278 \times 10^{-30}$	0.0122
$^{210}_{82}\text{Pb}$	3.790	16.57	$1.866 \times 10^{-17}$	$1.334 \times 10^{22}$	$0.959 \times 10^{21}$	$6.676 \times 10^{-37}$	0.0293
$^{188}_{84}\text{Po}$	8.087	-3.40	$1.733 \times 10^3$	$1.950 \times 10^{22}$	$1.452 \times 10^{21}$	$8.129 \times 10^{-17}$	0.0147
$^{190}_{84}\text{Po}$	7.693	-2.60	$2.772 \times 10^2$	$1.902 \times 10^{22}$	$1.411 \times 10^{21}$	$5.907 \times 10^{-18}$	0.0333
$^{192}_{84}\text{Po}$	7.319	-1.54	$2.392 \times 10^1$	$1.855 \times 10^{22}$	$1.371 \times 10^{21}$	$3.909 \times 10^{-19}$	0.0446
$^{194}_{84}\text{Po}$	6.990	-0.41	$1.782 \times 10^0$	$1.813 \times 10^{22}$	$1.335 \times 10^{21}$	$3.249 \times 10^{-20}$	0.0410
$^{196}_{84}\text{Po}$	6.660	0.76	$1.205 \times 10^{-1}$	$1.770 \times 10^{22}$	$1.299 \times 10^{21}$	$2.041 \times 10^{-21}$	0.0455
$^{198}_{84}\text{Po}$	6.310	2.18	$4.580 \times 10^{-3}$	$1.722 \times 10^{22}$	$1.259 \times 10^{21}$	$8.283 \times 10^{-23}$	0.0439
$^{200}_{84}\text{Po}$	5.980	3.79	$1.124 \times 10^{-4}$	$1.677 \times 10^{22}$	$1.222 \times 10^{21}$	$3.066 \times 10^{-24}$	0.0300
$^{202}_{84}\text{Po}$	5.700	5.13	$5.138 \times 10^{-6}$	$1.637 \times 10^{22}$	$1.188 \times 10^{21}$	$1.721 \times 10^{-25}$	0.0251
$^{204}_{84}\text{Po}$	5.480	6.28	$3.638 \times 10^{-7}$	$1.605 \times 10^{22}$	$1.161 \times 10^{21}$	$1.376 \times 10^{-26}$	0.0228
$^{206}_{84}\text{Po}$	5.330	7.15	$4.907 \times 10^{-8}$	$1.583 \times 10^{22}$	$1.141 \times 10^{21}$	$2.254 \times 10^{-27}$	0.0191
$^{208}_{84}\text{Po}$	5.220	7.97	$7.427 \times 10^{-9}$	$1.567 \times 10^{22}$	$1.126 \times 10^{21}$	$5.727 \times 10^{-28}$	0.0115
$^{210}_{84}\text{Po}$	5.407	7.08	$5.765 \times 10^{-8}$	$1.596 \times 10^{22}$	$1.142 \times 10^{21}$	$7.615 \times 10^{-27}$	0.0065
$^{212}_{84}\text{Po}$	8.950	-6.52	$2.295 \times 10^6$	$2.054 \times 10^{22}$	$1.466 \times 10^{21}$	$4.598 \times 10^{-14}$	0.0341
$^{214}_{84}\text{Po}$	7.830	-3.87	$5.138 \times 10^3$	$1.921 \times 10^{22}$	$1.366 \times 10^{21}$	$4.309 \times 10^{-17}$	0.0873
$^{216}_{84}\text{Po}$	6.900	-0.82	$4.580 \times 10^0$	$1.803 \times 10^{22}$	$1.278 \times 10^{21}$	$3.670 \times 10^{-20}$	0.0976
$^{218}_{84}\text{Po}$	6.110	2.27	$3.722 \times 10^{-3}$	$1.696 \times 10^{22}$	$1.199 \times 10^{21}$	$2.844 \times 10^{-23}$	0.1092
$^{198}_{86}\text{Rn}$	7.349	-1.19	$1.066 \times 10^1$	$1.859 \times 10^{22}$	$1.360 \times 10^{21}$	$9.928 \times 10^{-20}$	0.0790
$^{200}_{86}\text{Rn}$	7.040	0.0	$6.931 \times 10^{-1}$	$1.820 \times 10^{22}$	$1.326 \times 10^{21}$	$8.491 \times 10^{-21}$	0.0616
$^{202}_{86}\text{Rn}$	6.770	1.06	$6.037 \times 10^{-2}$	$1.785 \times 10^{22}$	$1.296 \times 10^{21}$	$9.713 \times 10^{-22}$	0.0480
$^{204}_{86}\text{Rn}$	6.550	2.00	$6.931 \times 10^{-3}$	$1.755 \times 10^{22}$	$1.270 \times 10^{21}$	$1.375 \times 10^{-22}$	0.0397
$^{206}_{86}\text{Rn}$	6.380	2.71	$1.352 \times 10^{-3}$	$1.733 \times 10^{22}$	$1.249 \times 10^{21}$	$2.830 \times 10^{-23}$	0.0382
$^{208}_{86}\text{Rn}$	6.260	3.34	$3.168 \times 10^{-4}$	$1.716 \times 10^{22}$	$1.233 \times 10^{21}$	$9.051 \times 10^{-24}$	0.0284
$^{210}_{86}\text{Rn}$	6.160	3.96	$7.600 \times 10^{-5}$	$1.703 \times 10^{22}$	$1.219 \times 10^{21}$	$3.957 \times 10^{-24}$	0.0158
$^{212}_{86}\text{Rn}$	6.380	3.17	$4.686 \times 10^{-4}$	$1.733 \times 10^{22}$	$1.237 \times 10^{21}$	$3.810 \times 10^{-23}$	0.0099
$^{214}_{86}\text{Rn}$	9.210	-6.57	$2.575 \times 10^6$	$2.084 \times 10^{22}$	$1.482 \times 10^{21}$	$4.350 \times 10^{-14}$	0.0399
$^{216}_{86}\text{Rn}$	8.200	-4.35	$1.552 \times 10^4$	$1.966 \times 10^{22}$	$1.393 \times 10^{21}$	$1.011 \times 10^{-16}$	0.1101
$^{218}_{86}\text{Rn}$	7.260	-1.45	$1.854 \times 10^1$	$1.850 \times 10^{22}$	$1.307 \times 10^{21}$	$1.226 \times 10^{-19}$	0.1220
$^{220}_{86}\text{Rn}$	6.400	1.75	$1.233 \times 10^{-2}$	$1.736 \times 10^{22}$	$1.223 \times 10^{21}$	$6.470 \times 10^{-23}$	0.1558
$^{222}_{86}\text{Rn}$	5.590	5.52	$2.093 \times 10^{-6}$	$1.733 \times 10^{22}$	$1.237 \times 10^{21}$	$1.055 \times 10^{-26}$	0.1743



TABLE II: Same as table 1, but for the even-even Ra, Th and U isotopes.

<i>Nuclei</i>	$Q_\alpha$ [MeV]	$\log_{10}(T_\alpha)$	$\lambda[s^{-1}]$	$v[fm/s]$	$\nu_0[s^{-1}]$	P	$P_0$
$^{202}_{88}\text{Ra}$	8.020	-2.58	$2.666 \times 10^2$	$1.943 \times 10^{22}$	$1.411 \times 10^{21}$	$2.931 \times 10^{-18}$	0.0645
$^{204}_{88}\text{Ra}$	7.636	-1.23	$1.174 \times 10^1$	$1.896 \times 10^{22}$	$1.372 \times 10^{21}$	$1.893 \times 10^{-19}$	0.0452
$^{206}_{88}\text{Ra}$	7.42	-0.62	$2.890 \times 10^0$	$1.869 \times 10^{22}$	$1.347 \times 10^{21}$	$3.750 \times 10^{-20}$	0.0572
$^{208}_{88}\text{Ra}$	7.27	0.15	$4.907 \times 10^{-1}$	$1.850 \times 10^{22}$	$1.329 \times 10^{21}$	$1.193 \times 10^{-20}$	0.0310
$^{210}_{88}\text{Ra}$	7.16	0.56	$1.909 \times 10^{-1}$	$1.836 \times 10^{22}$	$1.315 \times 10^{21}$	$5.682 \times 10^{-21}$	0.0256
$^{212}_{88}\text{Ra}$	7.03	1.15	$4.907 \times 10^{-2}$	$1.819 \times 10^{22}$	$1.298 \times 10^{21}$	$1.982 \times 10^{-21}$	0.0191
$^{214}_{88}\text{Ra}$	7.27	0.40	$2.759 \times 10^{-1}$	$1.851 \times 10^{22}$	$1.316 \times 10^{21}$	$1.575 \times 10^{-20}$	0.0133
$^{216}_{88}\text{Ra}$	9.53	-6.74	$3.809 \times 10^6$	$2.120 \times 10^{22}$	$1.503 \times 10^{21}$	$5.580 \times 10^{-14}$	0.0454
$^{218}_{88}\text{Ra}$	8.55	-4.59	$2.697 \times 10^4$	$2.008 \times 10^{22}$	$1.419 \times 10^{21}$	$2.049 \times 10^{-16}$	0.0928
$^{220}_{88}\text{Ra}$	7.60	-1.74	$3.809 \times 10^1$	$1.893 \times 10^{22}$	$1.333 \times 10^{21}$	$2.854 \times 10^{-19}$	0.1001
$^{222}_{88}\text{Ra}$	6.68	1.59	$1.782 \times 10^{-2}$	$1.774 \times 10^{22}$	$1.245 \times 10^{21}$	$1.269 \times 10^{-22}$	0.1127
$^{224}_{88}\text{Ra}$	5.79	5.53	$2.046 \times 10^{-6}$	$1.651 \times 10^{22}$	$1.155 \times 10^{21}$	$1.216 \times 10^{-26}$	0.1457
$^{226}_{88}\text{Ra}$	4.87	10.73	$1.291 \times 10^{-11}$	$1.514 \times 10^{22}$	$1.056 \times 10^{21}$	$5.861 \times 10^{-32}$	0.2086
$^{210}_{90}\text{Th}$	8.053	-1.77	$4.082 \times 10^1$	$1.948 \times 10^{22}$	$1.395 \times 10^{21}$	$9.009 \times 10^{-19}$	0.0325
$^{212}_{90}\text{Th}$	7.952	-1.44	$1.927 \times 10^1$	$1.935 \times 10^{22}$	$1.381 \times 10^{21}$	$4.616 \times 10^{-19}$	0.0302
$^{214}_{90}\text{Th}$	7.83	-1.00	$6.931 \times 10^0$	$1.921 \times 10^{22}$	$1.366 \times 10^{21}$	$1.978 \times 10^{-19}$	0.0257
$^{216}_{90}\text{Th}$	8.07	-1.55	$2.459 \times 10^1$	$1.950 \times 10^{22}$	$1.382 \times 10^{21}$	$1.256 \times 10^{-18}$	0.0142
$^{218}_{90}\text{Th}$	9.85	-7.00	$6.931 \times 10^6$	$2.156 \times 10^{22}$	$1.523 \times 10^{21}$	$7.388 \times 10^{-14}$	0.0616
$^{220}_{90}\text{Th}$	8.95	-5.01	$7.093 \times 10^4$	$2.055 \times 10^{22}$	$1.447 \times 10^{21}$	$5.102 \times 10^{-16}$	0.0961
$^{222}_{90}\text{Th}$	8.13	-2.55	$2.459 \times 10^2$	$1.958 \times 10^{22}$	$1.374 \times 10^{21}$	$2.514 \times 10^{-18}$	0.0712
$^{224}_{90}\text{Th}$	7.30	0.11	$5.381 \times 10^{-1}$	$1.855 \times 10^{22}$	$1.298 \times 10^{21}$	$4.512 \times 10^{-21}$	0.0919
$^{226}_{90}\text{Th}$	6.45	3.39	$2.824 \times 10^{-4}$	$1.743 \times 10^{22}$	$1.216 \times 10^{21}$	$1.901 \times 10^{-24}$	0.1221
$^{228}_{90}\text{Th}$	5.52	7.92	$8.333 \times 10^{-9}$	$1.612 \times 10^{22}$	$1.121 \times 10^{21}$	$5.626 \times 10^{-29}$	0.1321
$^{230}_{90}\text{Th}$	4.77	12.51	$2.142 \times 10^{-13}$	$1.498 \times 10^{22}$	$1.038 \times 10^{21}$	$1.203 \times 10^{-33}$	0.1714
$^{232}_{90}\text{Th}$	4.08	17.76	$1.205 \times 10^{-18}$	$1.385 \times 10^{22}$	$0.957 \times 10^{21}$	$4.447 \times 10^{-39}$	0.2831
$^{218}_{92}\text{U}$	8.773	-3.29	$1.358 \times 10^3$	$2.034 \times 10^{22}$	$1.437 \times 10^{21}$	$3.036 \times 10^{-17}$	0.0311
$^{220}_{92}\text{U}$	10.30	-7.22	$1.156 \times 10^7$	$2.205 \times 10^{22}$	$1.553 \times 10^{21}$	$1.700 \times 10^{-13}$	0.0438
$^{224}_{92}\text{U}$	8.620	-3.15	$9.904 \times 10^2$	$2.016 \times 10^{22}$	$1.411 \times 10^{21}$	$1.389 \times 10^{-17}$	0.0505
$^{226}_{92}\text{U}$	7.701	-0.30	$1.386 \times 10^0$	$1.906 \times 10^{22}$	$1.329 \times 10^{21}$	$1.900 \times 10^{-20}$	0.0549
$^{228}_{92}\text{U}$	6.80	2.76	$1.205 \times 10^{-3}$	$1.790 \times 10^{22}$	$1.245 \times 10^{21}$	$9.088 \times 10^{-24}$	0.1065
$^{230}_{92}\text{U}$	5.99	6.43	$2.575 \times 10^{-7}$	$1.680 \times 10^{22}$	$1.164 \times 10^{21}$	$1.914 \times 10^{-27}$	0.1155
$^{232}_{92}\text{U}$	5.41	9.52	$2.093 \times 10^{-10}$	$1.596 \times 10^{22}$	$1.103 \times 10^{21}$	$1.360 \times 10^{-30}$	0.1395
$^{234}_{92}\text{U}$	4.86	13.02	$6.620 \times 10^{-14}$	$1.512 \times 10^{22}$	$1.042 \times 10^{21}$	$4.166 \times 10^{-34}$	0.1525
$^{236}_{92}\text{U}$	4.57	14.99	$7.093 \times 10^{-16}$	$1.466 \times 10^{22}$	$1.007 \times 10^{21}$	$3.976 \times 10^{-36}$	0.1771
$^{238}_{92}\text{U}$	4.27	17.27	$3.722 \times 10^{-18}$	$1.417 \times 10^{22}$	$0.970 \times 10^{21}$	$1.572 \times 10^{-38}$	0.2440

TABLE III: Same as table 1, but for the even-even superheavy nuclei.

<i>Nuclei</i>	$Q_\alpha$ [MeV]	$T_\alpha$	$\lambda$	$v$ [fm/s]	$\nu_0$ [s <sup>-1</sup> ]	P	P <sub>0</sub>
<sup>294</sup> 118	11.81	0.89 ms	$7.788 \times 10^2$	$2.365 \times 10^{22}$	$1.502 \times 10^{21}$	$9.304 \times 10^{-17}$	0.0056
<sup>292</sup> 116	10.66	18 ms	$3.851 \times 10^1$	$2.246 \times 10^{22}$	$1.430 \times 10^{21}$	$5.394 \times 10^{-19}$	0.0499
<sup>290</sup> 116	11.00	7.1 ms	$9.763 \times 10^1$	$2.282 \times 10^{22}$	$1.457 \times 10^{21}$	$3.813 \times 10^{-18}$	0.0176
<sup>288</sup> 114	10.09	0.80 s	$8.664 \times 10^{-1}$	$2.185 \times 10^{22}$	$1.398 \times 10^{21}$	$5.734 \times 10^{-20}$	0.0108
<sup>286</sup> 114	10.33	0.13 s	$5.331 \times 10^0$	$2.153 \times 10^{22}$	$1.418 \times 10^{21}$	$2.476 \times 10^{-19}$	0.0152
<sup>270</sup> Ds	11.20	0.1 ms	$6.931 \times 10^3$	$2.302 \times 10^{22}$	$1.507 \times 10^{21}$	$3.486 \times 10^{-16}$	0.0132
<sup>266</sup> Hs	10.34	2.3 ms	$3.014 \times 10^2$	$2.211 \times 10^{22}$	$1.456 \times 10^{21}$	$1.134 \times 10^{-17}$	0.0183
<sup>264</sup> Hs	10.58	0.25 ms	$2.759 \times 10^3$	$2.237 \times 10^{22}$	$1.476 \times 10^{21}$	$4.143 \times 10^{-17}$	0.0451
<sup>266</sup> Sg	8.76	33.88 s	$2.046 \times 10^{-2}$	$2.035 \times 10^{22}$	$1.339 \times 10^{21}$	$1.473 \times 10^{-21}$	0.0104
<sup>260</sup> Sg	9.93	8.51 ms	$8.144 \times 10^1$	$2.167 \times 10^{22}$	$1.438 \times 10^{21}$	$3.359 \times 10^{-18}$	0.0169